Journal of Geoscience and Environment Protection, 2026, 14(7), 223-248
https://www.scirp.org/journal/gep
ISSN Online: 2327-4344
ISSN Print: 2327-4336

Granulometric and Facies Analysis of Sandstone Reservoir of the Y-Field in the Tano Basin, Ghana

Asare Asante-Annor[1*], Ebenezer Ansah[1], Priscilla Efua Baiden[1], Clement Nuamah[2], Mark Prempeh[3]

[1]Geological Engineering Department, University of Mines and Technology, Tarkwa, Ghana
[2]Geophysics Department, Ghana National Petroleum Corporation, Tema, Ghana
[3]Exploration and Appraisal, Ghana National Petroleum Corporation, Tema, Ghana
Email: *aasante-annor@umat.edu.gh

How to cite this paper: Asante-Annor, A., Ansah, E., Baiden, P. E., Nuamah, C., & Prempeh, M. (2026). Granulometric and Facies Analysis of Sandstone Reservoir of the Y-Field in the Tano Basin, Ghana. *Journal of Geoscience and Environment Protection, 14,* 223-248.
https://doi.org/10.4236/gep.2026.147014

Received: July 6, 2026
Accepted: July 21, 2026
Published: July 24, 2026

Copyright © 2026 by author(s) and Scientific Research Publishing Inc.
This work is licensed under the Creative Commons Attribution International License (CC BY 4.0).
http://creativecommons.org/licenses/by/4.0/
Open Access

Abstract

Grain size analysis is an essential sedimentological tool for determining hydrodynamic conditions, mode of transport and deposition of detrital sediments. In this study, detailed grain size analysis was conducted using fifty-six sieve analysis samples acquired from a total of three well core data (WX, WY and WZ) in order to determine the depositional environment of the Y-Field in the Jubilee Field, a hydrocarbon reservoir, supported by facies analysis. Depositional environments, hydrodynamic conditions and mode of sediment transport were determined using bivariate plots and linear discriminate function (LDF) analysis. The results reveal that the unit consists of medium to silt sands with majority being poorly sorted. The sediments have a unimodal distribution of 2ϕ and 1ϕ, while few beds have a bimodal of 3ϕ, 4ϕ, 5ϕ, 6ϕ, 7ϕ and 8ϕ. The unit has near symmetrical to very fine skewed but mostly platykurtic to very leptokurtic sediments. Bivariate plots of the statistical measures show that the depositional environments were impacted mostly by river conditions. Additionally, the cumulative frequency curves show that the majority of the sediments were transported via saltation while fine grains were transported by suspension and a few indications of the traction process. The sediment classification ternary diagram reveals that 44% of the samples are silty sand, 22% sandy silt and 6% sand per the fine plot. For the coarse plot, most of the samples (22%) are slightly gravelly sand with one sample (6%) being gravelly muddy sand. The Shepard 1954 classification revealed for the coarse plot as sand, silt and clay which is about 28%. Most of the samples (50%) grouped in the sand region and few others (22%) in the silty sand and sandy silt regions (22%) in the fine plot. The results of the LDF analysis are mainly indicative of shallow marine, beach, turbidity current and fluvial environments.

Keywords

Granulometric Analysis, Sediment Classification, Grain Size, Facies Analysis

1. Introduction

Grain size is a significant physical characteristic of sediments and is essential to understand the inherent characteristics and dynamic forces at play during deposition. Likewise, grain size metrics aid in investigating the provenance (origin) of sediments, environment of deposition, textural classification of sedimentary rocks and the energy flux of different mechanisms that transported the sediments (Ghaznavi et al., 2019). Prior to final induration, clastic rock grain size metrics provide precise information on the transport, sorting, and depositional conditions of the sediment (Baiyegunhi et al., 2020). For a deeper comprehension of depositional environments, studying other sedimentological factors, such as sedimentary structures and their relationships, palaeocurrent, geometry, and fossil content, becomes necessary in addition to particle size analysis. This is because these parameters are more dependent on the mechanisms in place during sediment deposition (Ghaznavi et al., 2019).

The exploration phase for commercial reserves necessitates a comprehension of the mechanisms of deposition of the petroleum play system in order to determine whether a suitable reservoir rock is likely to have formed (Nichols, 2009). The grain size of minerals is dependent on the kind of depositional environment, medium of transport, the duration and distance of transportation and the predominate depositional conditions which serves as an environmental indicator (Kanhaiya et al., 2017; López, 2017; Ocheli et al., 2018). The facies of the reservoir are determined by the grain-size distribution and its relationship has a significant impact on hydrocarbon and water circulation within the reservoir unit. As a result, this component of sedimentological study is critical for well planning and effective reservoir management (Ogbe, 2021).

Grain-size distribution, including the frequency of stacking patterns and accumulations of a sand-body's complexity, produces a high level of reservoir variability which differs depending on the environment of deposition (Ogbe, 2021). The level of complexity and variability introduces uncertainty in estimating sand connectivity and creates difficulties in hydrocarbon extraction techniques (Ogbe, 2021). To overcome these difficulties, an in-depth knowledge of the size distribution of grains and environment of deposition, as well as the depositional processes that occur throughout reservoir development, is essential (Ogbe, 2021).

Ansah et al. (2022) characterised the depositional setting of the Jubilee Field reservoir system; however, a comprehensive and thorough textural investigation was not well highlighted. Therefore, this research aims to examine the sedimentological characteristics of the Jubilee Field reservoir system using grain size analysis dataset. This study will focus on the use of sieve analysis to examine depositional characteristics and its potential impacts on reservoir quality. This work seeks to use detailed grain size analysis to deduce the depositional environment of the reservoir system.

2. Study Location

The area of study is situated in the Jubilee Field (**Figure 1**) which is located 60 km offshore between the West Cape Three Points and the Deepwater Tano blocks in Ghana. It is situated at a water depth of 1100 m (Anon, 2009; TGL, 2019).

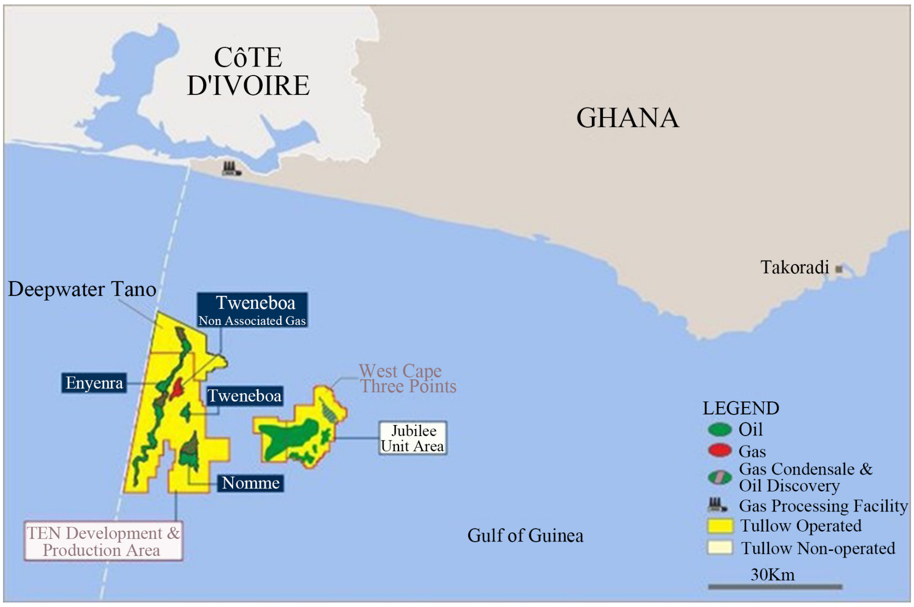

Source: TGL, 2019.

Figure 1. Location map of the study area.

3. Stratigraphical Setting

Tano Basin is an offshore basin and a member of the West African Transform Margin basin complex that is located in southwest Ghana (Bempong et al., 2019). It is largely offshore and a smaller portion onshore. The Tano Basin encompasses three oil fields which includes; the Jubilee field, Tweneboa Enyenra and Ntomme (TEN) oil field and Sankofa Gye Nyame field (Bempong et al., 2022). The Romanche and St. Paul transform zones comprises its eastern and western boundaries, the ocean and the African continent, its southern and northern boundaries, respectively. During the Mesozoic Era, rifting caused it to modify into a pull-apart basin (Atta-Peters et al., 2013).

According to Bempong et al. (2021), as the South Atlantic Ocean widened and grew deeper, subsequent rift system expansion and subsidence thinned the crust of the continent and developed openings for lithic fill to enter the basin. The lithic fill of the basin started within the Aptian (**Figure 2**, **Figure 3**) with substantial continental clastic from the rivers Tano and Ankobra. On the other hand, the basin is altered by wrench tectonics in the Cretaceous through an extensive transform fault characterised by fracture and sagging (Rupke et al., 2010). The undersea canyon system acted as a clastic material delivery channel into the Tano Basin (Daily et al., 2013). Four patterns (**Figure 2**), which are listed below, describe the relation between tectonic periods and related sedimentation:

1) Paleozoic to Lower Mesozoic strata were identified as the pre-rift stage of a stable platform.

2) The syn-rift stage, which started in the Jurassic and advanced into the Early Cretaceous was characterised by a continental separation between South America and Africa. The separation forced the continental boundary to be in a transpressional setting as evidenced by the number of folds and flow features in the basin. These data suggest that the continental margin contributed in the total shearing of the two plates (Ansah et al., 2022).

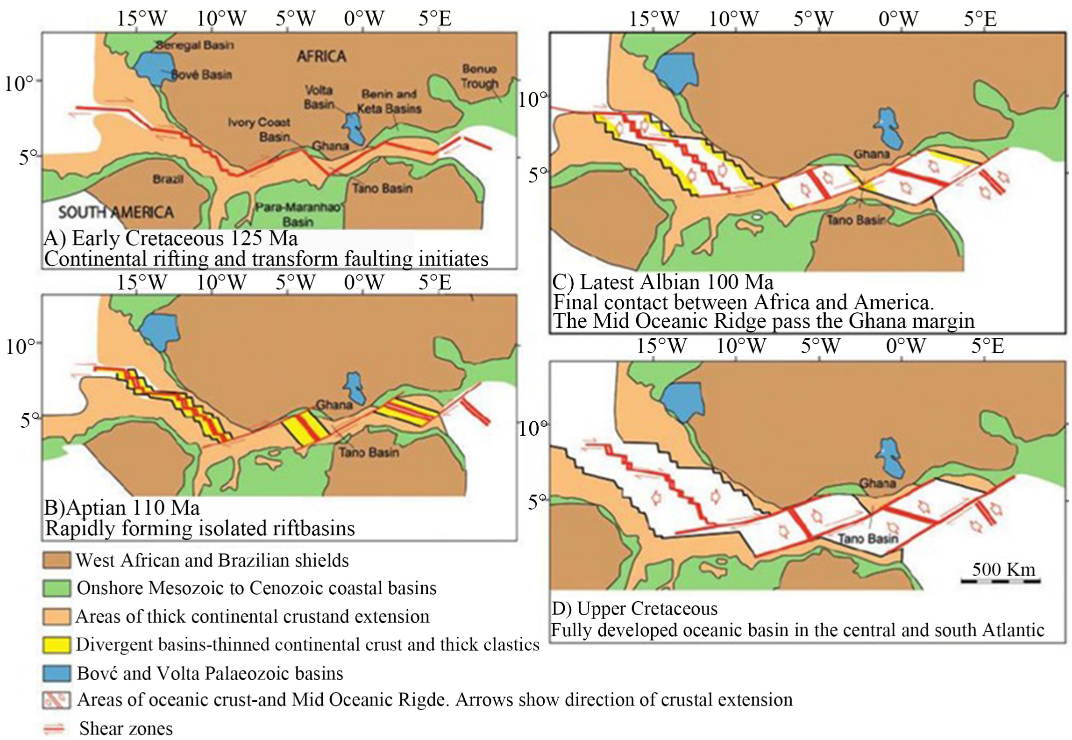

Source: Rupke et al., 2010.

Figure 2. Geological setting of the study area.

3) The top syn-rift unconformity depicts the climax of a time of rapid continental separation and distortion. An apparent angular unconformity over the continental platform, as shown on the seismic profile by a Top Syn-rift reflection, distinguishes it. The most recent continental collision of the two plates, which happened in the late Albian or early Cenomanian marks the unconformity. The occurrence of thermal rising of the outer margins of Ghana towards the end of the

Albian is likely to correlate with magnetic under plating noted in deep magnetic data and seismic gravity along the margin (Antobreh et al., 2009).

4) After the ultimate separation of the African and American plates, marine deposition that occurred from the Cenomanian to the recent depicts the post-rift stage. During this era, large-scale ocean transforms faults (Romanche and St. Paul) formed across the path of the earlier continental transforms. Despite the possibility of some deformation continuing beyond the margins of the continents, the final separation typically indicates a period of thermal and rapid subsidence.

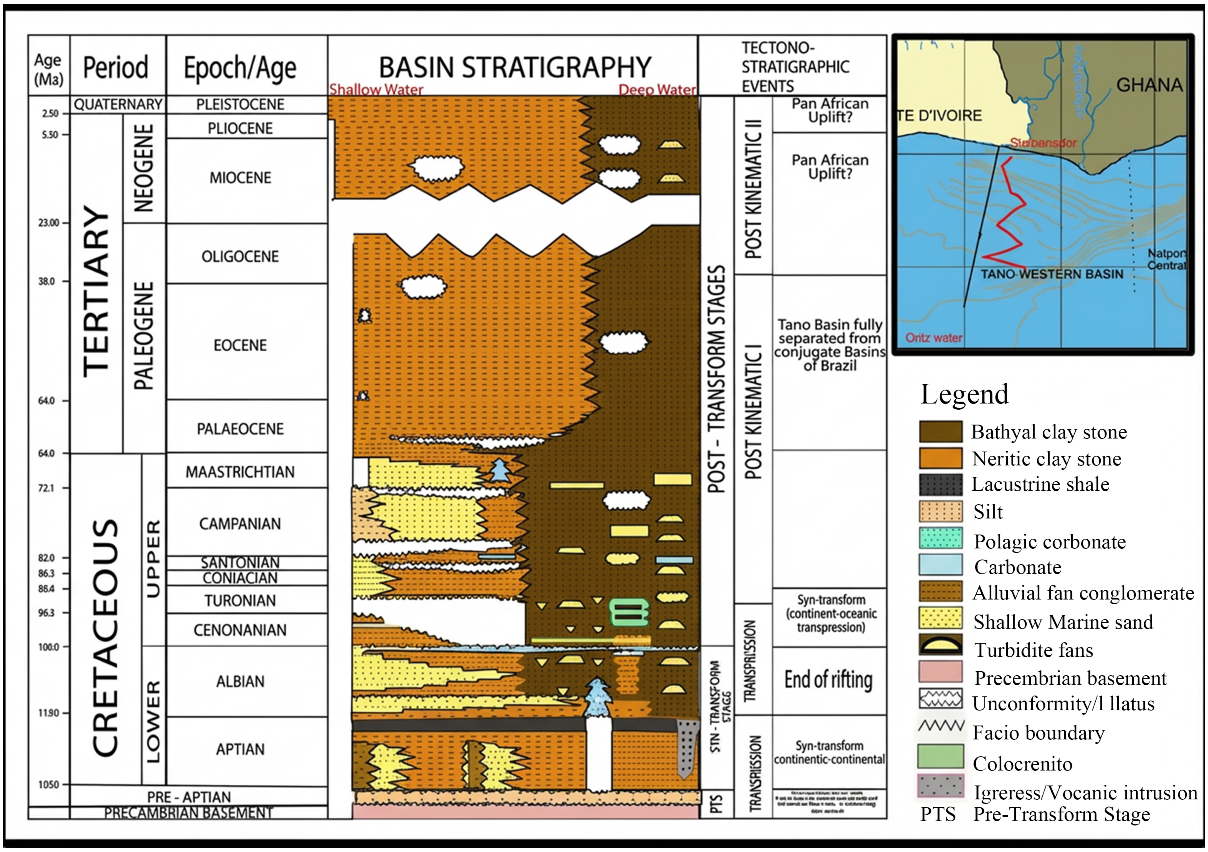

Source: Bempong et al., 2022.

Figure 3. Chronostratigraphic summary of the study area.

4. Materials and Methods

A total of two well core data (WY and WZ) comprising of one hundred and forty-one sieve analysis samples were used for detailed granulometric analysis. The samples cover depths ranging from 3175.60 m to 3506.60 m and represents 18 sedimentary facies. The number of samples obtained from each facies reflects its occurrence within the cored intervals. During data analysis, samples exhibiting the same lithofacies and similar depositional characteristics were grouped into 18 facies (Table 1). These groups represent statistically and sedimentologically comparable intervals and were used for subsequent grain-size and reservoir quality analysis to facilitate interpretation.

Table 1. Summary table of the depositional facies.

Well	Depth (m)	Facies	Number of Samples
WX	3421.50 - 3474.80	Dewatered/deformed sandstone (Sd)	8
	3465.50 - 3503.91	Sandy heterolithics (Hs)	5
	3298.10 - 3410.50	Pebbly sandstone (Sc)	22
	3401.50 - 3466.50	Mudstone (M)	7
	3393.50 - 3492.70	Irregularly laminated heterolithics (Hi)	10
	3394.50 - 3462.54	Slump deformed mudstones/heterolithics (MHd)	5
	3396.50 - 3483.50	Muddy debrite (Dm)	7
	3403.05 - 3404.20	Planar laminated heterolithics (Hp)	2
	3406.25 - 3504.50	Ripple cross-laminated sandstone (Sxr)	5
	3407.42 - 3484.25	Structureless sandstone (Ss)	11
	3408.50 - 3502.50	Planar stratified sandstone (Sp)	9
	3414.50 - 3479.50	Sandy debrite (Ds)	4
	3419.05 - 3499.50	Weakly stratified sandstone (Sm)	5
	3425.50 - 3434.50	Conglomerate (Cgl)	6
	3439.50 - 3495.50	Bioturbated sandstone (Sb)	2
	3450.57	Injectite (I)	1
	3468.50 - 3505.50	Bioturbated heterolithics (Hb)	15
	3500.55 - 3506.60	Fine grained sandstone (Sf)	5
WY	3175.6 - 3188.30	Dewatered/deformed sandstone (Sd)	2
	3231.3	Sandy heterolithics (Hs)	1
	3250.4 - 3298.10	Pebbly sandstone (Sc)	5
	3337.3	Mudstone (M)	1
	3234 - 3422.40	Structureless sandstone (Ss)	3
Total			**141**

For the statistical analysis, a scale proposed by Krumbein and Monk (1943) based on the following relationship was used:

$$\phi = -\log_2(D) \tag{1}$$

where ϕ is phi size and D is the grain diameter in millimeters.

Plots of cumulative frequency curves were plotted versus the grain sizes in ϕ unit to identify the $\phi 5$, $\phi 16$, $\phi 25$, $\phi 50$, $\phi 75$, $\phi 84$ and $\phi 95$ percentiles and then the statistical measures which includes mean, standard deviation, skewness, and kurtosis, were calculated using both the graphical and moment methods. The statistical measurement for the graphical method which have been verified by Folk and Ward (1957) is defined as follows:

$$\text{Graphic Mean,} \quad M_Z = \frac{\phi_{16} + \phi_{50} + \phi_{84}}{3} \tag{2}$$

$$\text{Inclusive Graphic Standard Deviation,}\quad \sigma_i = \frac{\phi_{84}-\phi_{16}}{4} + \frac{\phi_{95}-\phi_5}{6.6} \tag{3}$$

$$\text{Inclusive Graphic Skewness,}\quad SK_t = \frac{\phi_{84}+\phi_{16}-2\phi_{50}}{2(\phi_{84}-\phi_{16})} + \frac{\phi_{95}+\phi_5-2\phi_{50}}{2(\phi_{95}-\phi_5)} \tag{4}$$

$$\text{Graphic Kurtosis,}\quad K_G = \frac{\phi_{95}-\phi_5}{2.44(\phi_{75}-\phi_{25})} \tag{5}$$

The statistical measurement for the moment method which have been verified by Krumbein and Pettijohn (1938) is as follows:

$$\text{Mean (1}^{\text{st}}\text{ Moment),}\quad \bar{X}_\phi = \frac{\sum fm}{n} \tag{6}$$

$$\text{Standard Deviation (2}^{\text{nd}}\text{ Moment),}\quad \sigma_\phi = \sqrt{\frac{\sum f\left(m-\bar{X}_\phi\right)^2}{100}} \tag{7}$$

$$\text{Skewness (3}^{\text{rd}}\text{ Moment),}\quad Sk_\phi = \frac{\sum f\left(m-\bar{X}_\phi\right)^3}{100{\sigma^3}_\phi} \tag{8}$$

$$\text{Kurtosis (4}^{\text{th}}\text{ Moment),}\quad K_\phi = \frac{\sum f\left(m-\bar{X}_\phi\right)^4}{100\sigma_\phi^4} \tag{9}$$

where f = weight percent (frequency) in each grain-size grade present;

m = midpoint of each grain-size grade in phi values;

n = total number in sample; 100 when f is in percent.

Sediment classification analysis was done to classify the samples using a classification scheme from (Folk, 1954, 1974) and (Shepard, 1954) produced by program SEDPLOT in **Figure 4** (Poppe & Eliason, 2008).

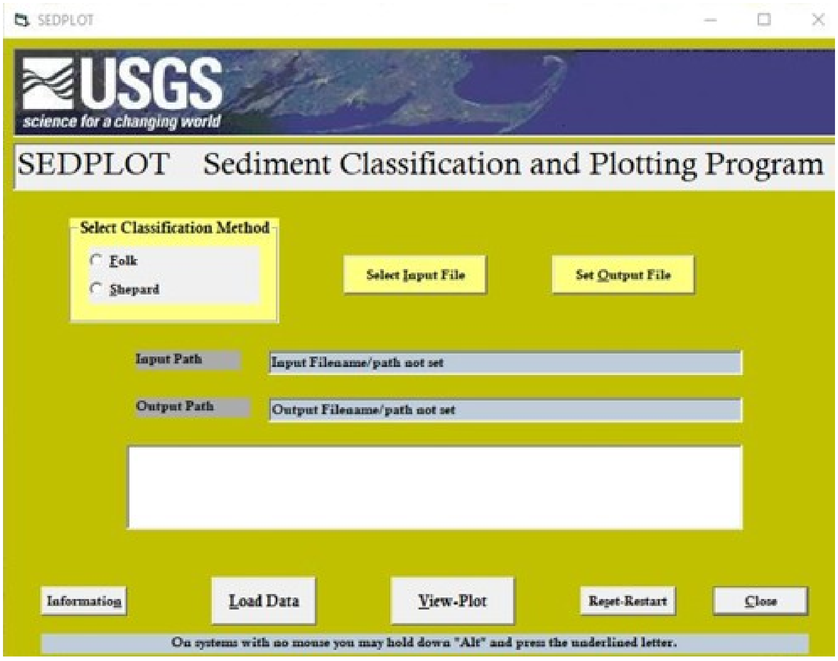

Figure 4. Window for SEDPLOT program.

The GSSTAT software (Figure 5) was used to generate statistics to characterise sediment grain-size distribution using the method of moments (Poppe et al., 2004).

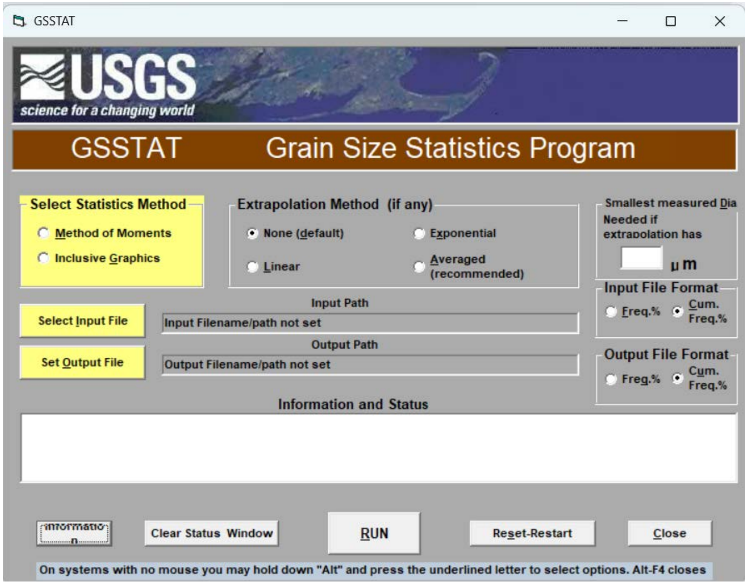

Figure 5. Window for GSSTAT program.

Bivariate plots were plotted between the different statistical parameters to establish the interrelationships between depositional settings according to the variation in the sediment textures (Ghaznavi et al., 2019). Linear discriminate function (LDF) analysis was further used to discriminate and interpret the depositional processes and environments using the following equations as established by Sahu, 1964:

- To distinguish between the aeolian and beach environments

$$Y_1 = -3.5688M_Z + 3.7016\sigma_i^2 - 2.0766SK_t + 3.1135K_G \quad (10)$$

For beach environment Y_1 is greater than −2.7411 and for aeolian environment Y_1 is less than −2.7411.

- To delineate between beach and shallow-marine environment

$$Y_2 = 15.6534M_Z + 65.7091\sigma_i^2 + 18.1071SK_t + 18.5043K_G \quad (11)$$

For beach environment Y_2 is less than 63.3650 and for shallow-marine environment Y_2 is greater than 63.3650.

- The following equation distinguishes the shallow-marine and fluvial settings

$$Y_3 = 0.2852M_Z - 8.7604\sigma_i^2 - 4.8932SK_t + 0.0482K_G \quad (12)$$

For shallow-marine environment Y_3 is greater than −7.4190 and for fluvial environment Y_3 is less than −7.4190.

- The following equation distinguishes the fluvial and marine turbidity environments

$$Y_4 = 0.7215M_Z - 0.40304\sigma_i^2 + 6.7322SK_t + 5.2927K_G \quad (13)$$

For marine turbidity environment Y_4 is greater than 10.000 and for fluvial environment Y_4 is less than 10.000.

5. Rationale and Interpretive Limits of the Bivariate and LDF Discriminants

The bivariate schemes of Friedman (1961, 1967) and the linear discriminant functions of Sahu (1964) were calibrated on grain-size populations from beach, dune, fluvial, shallow-marine and turbidity-current sands, where sorting, skewness and kurtosis reflect differences in traction, saltation and suspension transport. The grain-size moments are used here for the detrital (heterolithic), debrite, structureless, stratified and slumped sandstone/mudstone facies of the study interval, because of the fact that these are grain-populations transported and reworked by the same basic mechanism (traction, saltation, suspension and gravity-flow support) and because of this, the moments of the grain-size are still informative in the relative dominance of these processes even though the facies were deposited by sediment gravity-flow rather than by the steady, unidirectional or wave-driven currents on which the discriminants were originally built (Sahu, 1964; Friedman, 1967; Kanhaiya et al., 2017). This is a continuation of existing practice in granulometric facies studies of ancient, gravity-flow-influenced reservoir sandstones, in which the same bivariate and LDF schemes are employed as a first order textural screen as well as in conjunction with core description rather than as a standalone indicator of environment (Ghaznavi et al., 2019; Baiyegunhi et al., 2020).

The use of these discriminants in a deep-water, gravity-flow dominated reservoir has definite interpretive limitations, however. The bivariate plots (Friedman 1961, 1967) and associated Y1 - Y4 linear discriminant function equations (Sahu 1964), do not incorporate an explicit debris-flow or hybrid-flow category, and therefore remobilised, poorly sorted deposits (such as debris flows, slumped heterolithics, and injectites) are not distinguished as a genetically distinct class in the classification scheme. Rather, based exclusively on the bulk grain-size statistics, such deposits are assigned to whichever pure end-member facies (beach, shallow-marine, fluvial, or turbidite) they most closely approximate. Bioturbation, dewatering and soft-sediment deformation can occur in these facies as post-depositional overprints, altering the primary grain-size distribution without being related to the depositional process, and so may lead to a bias in the computed shape parameters, skewness, kurtosis and Y-values. The Friedman (1961, 1967) and Sahu (1964) calibration datasets are from modern, unconsolidated, shallow, current or wave-dominated sediments, so the labels of the environment are used as indicative only, and are interpreted here only in conjunction with the core sedimentological description.

6. Results and Discussion

6.1. Frequency Curves

Frequency distribution curves from the three wells (WX, WY and WZ) indicate the distribution of the descriptive statistical curves for the three wells and show peak constituents and uniformity of sediment fraction for the study location (**Figure 6**). The curves are primarily unimodal with a dominating peak around 2ϕ (**Figure 6(F)**) and 1ϕ (**Figure 6(J)** and **Figure 6(K)**), whereas, a few of the samples exhibit bimodal behaviour with distinct peaks at 3ϕ (**Figure 6(C)**, **Figure 6(D)**, **Figure 6(H)**, **Figure 6(G)**, **Figure 6(J)-(O)**), 4ϕ (**Figures 6(A)-(G)**, **Figuress 6(P)-(Q)**), 5ϕ (**Figure 6(E)**, **Figure 6(K)**, **Figure 6(O)** and **Figure 6(P)**), 6ϕ (**Figure 6(H)**, **Figure 6(J)**, **Figure 6(K)**, **Figure 6(M)** and **Figure 6(N)**), 7ϕ (**Figures 6(A)-(L)**, **Figures 6(O)-(R)**) and 8ϕ (**Figure 6(D)**). This is explained by the occurrence of both unimodal and bimodal populations, indicating the presence of both types of sediments (i.e., pure sand without any silt particles and sand mixed with some finer particles). For sediments depicting unimodality, sediments settled throughout a uniform depositional process. Bimodality is attributed to the mixing of populations of various sizes from the source areas, variations in the velocities of depositional, or differences in the modes of transportation, such as rolling, saltation, or suspension (Ghaznavi et al., 2019). The bimodality is also most likely as a result of the low energy present during sediment deposition.

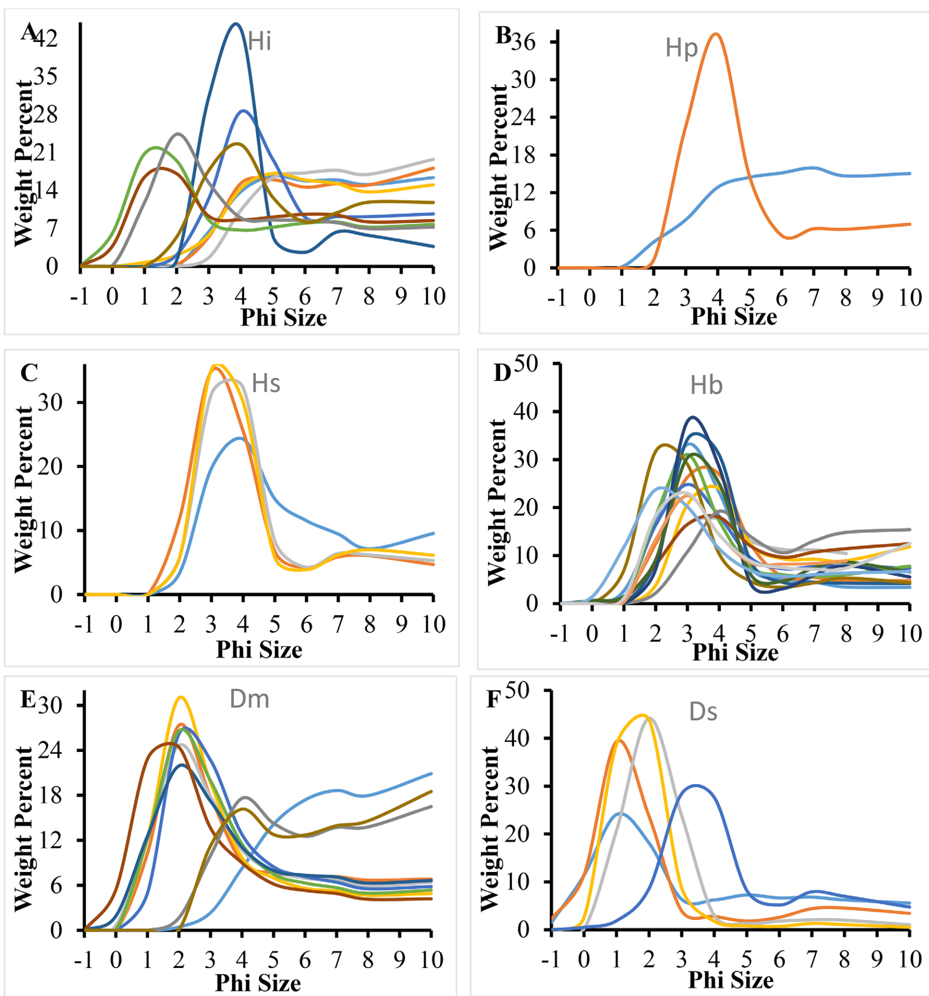

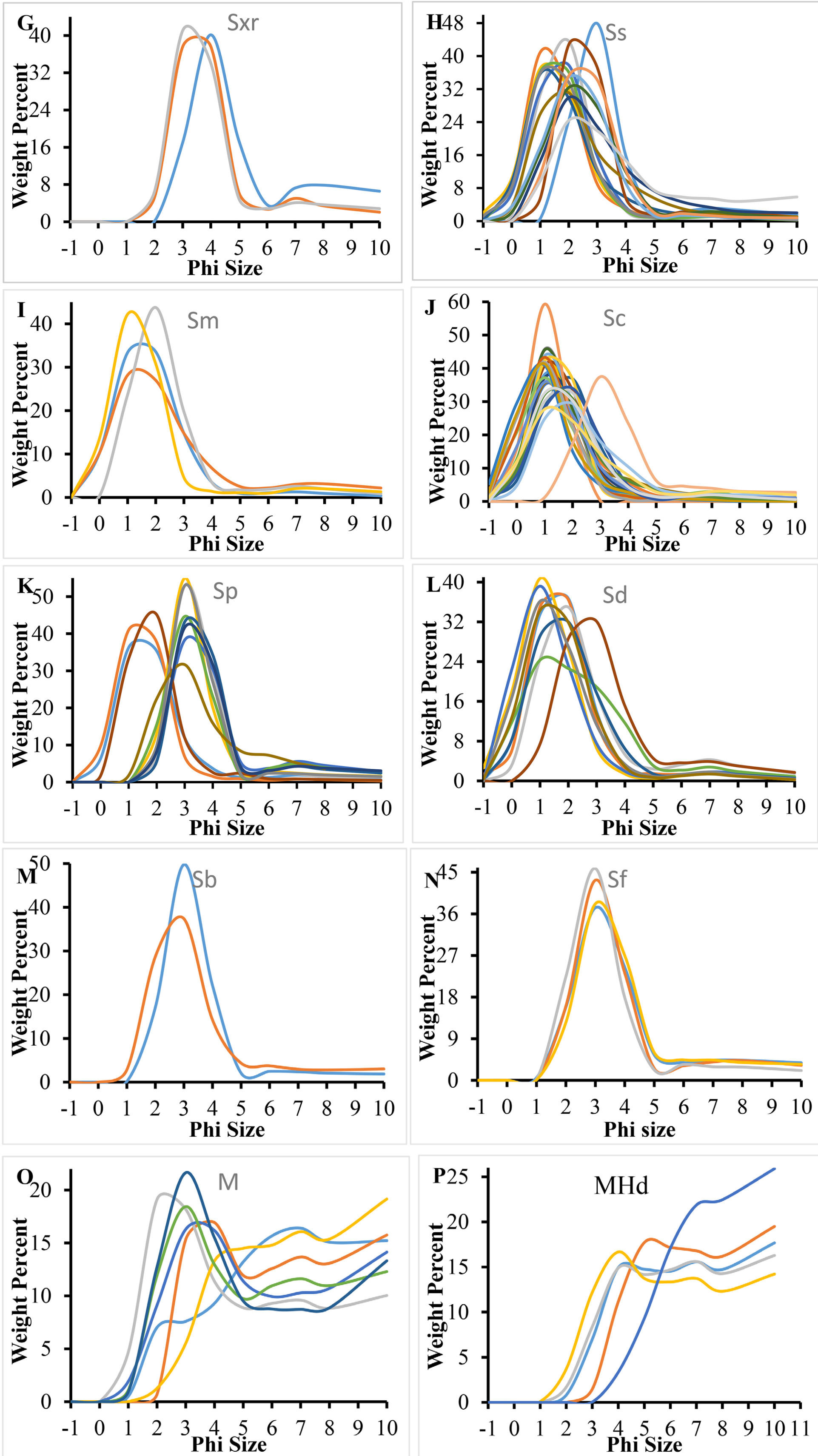
G
Sxr
Weight Percent
Phi Size
H
Ss
Weight Percent
Phi Size
I
Sm
Weight Percent
Phi Size
J
Sc
Weight Percent
Phi Size
K
Sp
Weight Percent
Phi Size
L
Sd
Weight Percent
Phi Size
M
Sb
Weight Percent
Phi Size
N
Sf
Weight Percent
Phi size
O
M
Weight Percent
Phi Size
P
MHd
Weight Percent
Phi Size

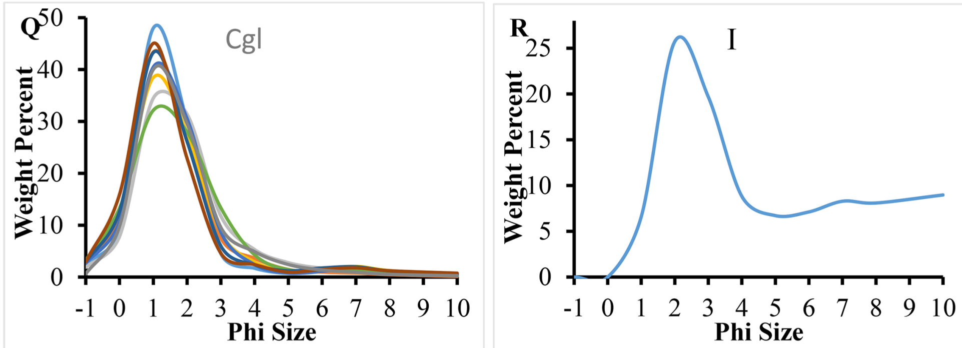

Figure 6. Frequency distribution curves for facies of the study area: A) IRregularly Laminated Heterolithics, B) Planar Laminated Heterolithics, C) Sandy Heterolithics, D) Bioturbated Heterolithics, E) Muddy Debrite, F) Sandy Debrite, G) Ripple Cross-Laminated Sandstone, H) Structureless Sandstone, I) Weakly Stratified Sandstone, J) Pebbly Sandstone, K) Planar Stratified Sandstone, L) Dewatered/Deformed Sandstone, M) Bioturbated Sandstone, N) Fine Grained Sandstone, O) Mudstone, P) Slump Deformed Mudstones/Heterolithics, Q) Conglomerate and R) Injectite.

6.2. Cumulative Frequency Curves

Additionally, phi values were plotted against the cumulative frequencies. The cumulative frequency plot highlights the various ways that the sediments were transported and deposited as well as their significance in the origin of the rock samples. The curve typically exhibited an S-shaped pattern when plotted on an arithmetic scale (**Figure 7**) and the slope of the central portion of the curve can be used to predict sorting. Low velocity and rapid rate of deposition leads to poor sorting and a broader and gentle slope in the distribution curves. In contrast, a very steep slope is an indication of good sorting (Ghaznavi et al., 2019; Oyanyan & Olugun, 2023; Cheng et al., 2023; Atat et al., 2022). From the cumulative frequency curves, the samples are predominantly silt, with few samples being medium to fine grain and very few being coarse in nature. The broadness and gentleness of the slope indicates that the grains are poorly sorted to very poorly sort (**Figure 7**). The cumulative frequencies also revealed that most of the sediments was transported by the process of saltation which is dependent on the rate of deposition followed by suspension population which reflects conditions above the depositional interface (Visher, 1969) and a few indications of the traction process.

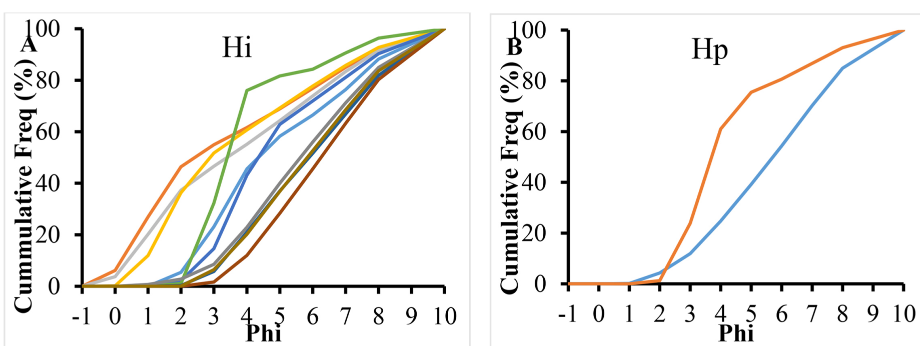

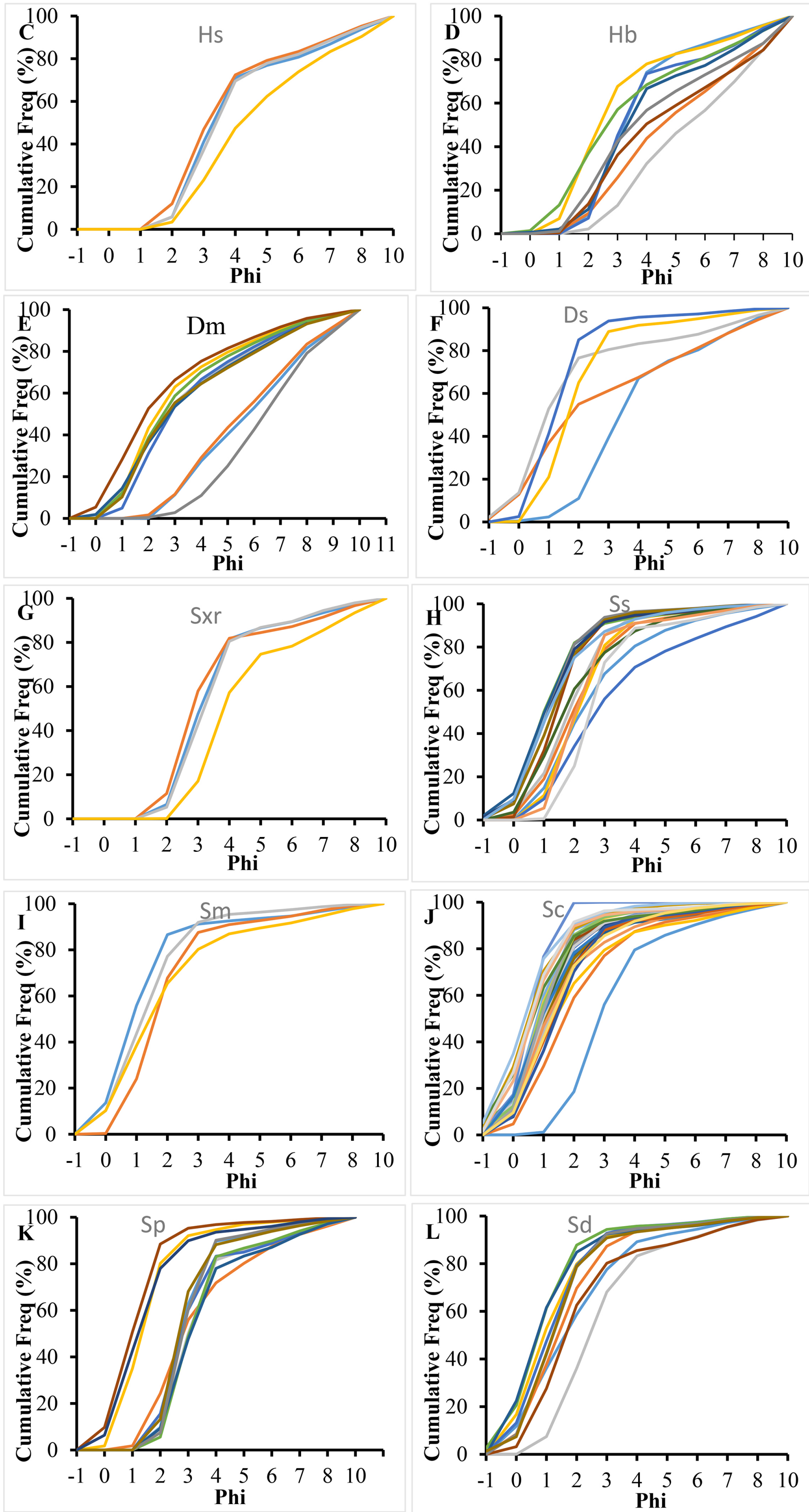
C
Hs
Cumulative Freq (%)
0
20
40
60
80
100
-1 0 1 2 3 4 5 6 7 8 10
Phi
D
Hb
Cumulative Freq (%)
-1 0 1 2 3 4 5 6 7 8 10
Phi
E
Dm
Cumulative Freq (%)
-1 0 1 2 3 4 5 6 7 8 9 10 11
Phi
F
Ds
Cumulative Freq (%)
-1 0 1 2 3 4 5 6 7 8 10
Phi
G
Sxr
Cumulative Freq (%)
-1 0 1 2 3 4 5 6 7 8 10
Phi
H
Ss
Cumulative Freq (%)
-1 0 1 2 3 4 5 6 7 8 10
Phi
I
Sm
Cumulative Freq (%)
-1 0 1 2 3 4 5 6 7 8 10
Phi
J
Sc
Cumulative Freq (%)
-1 0 1 2 3 4 5 6 7 8 10
Phi
K
Sp
Cumulative Freq (%)
-1 0 1 2 3 4 5 6 7 8 10
Phi
L
Sd
Cumulative Freq (%)
-1 0 1 2 3 4 5 6 7 8 10
Phi

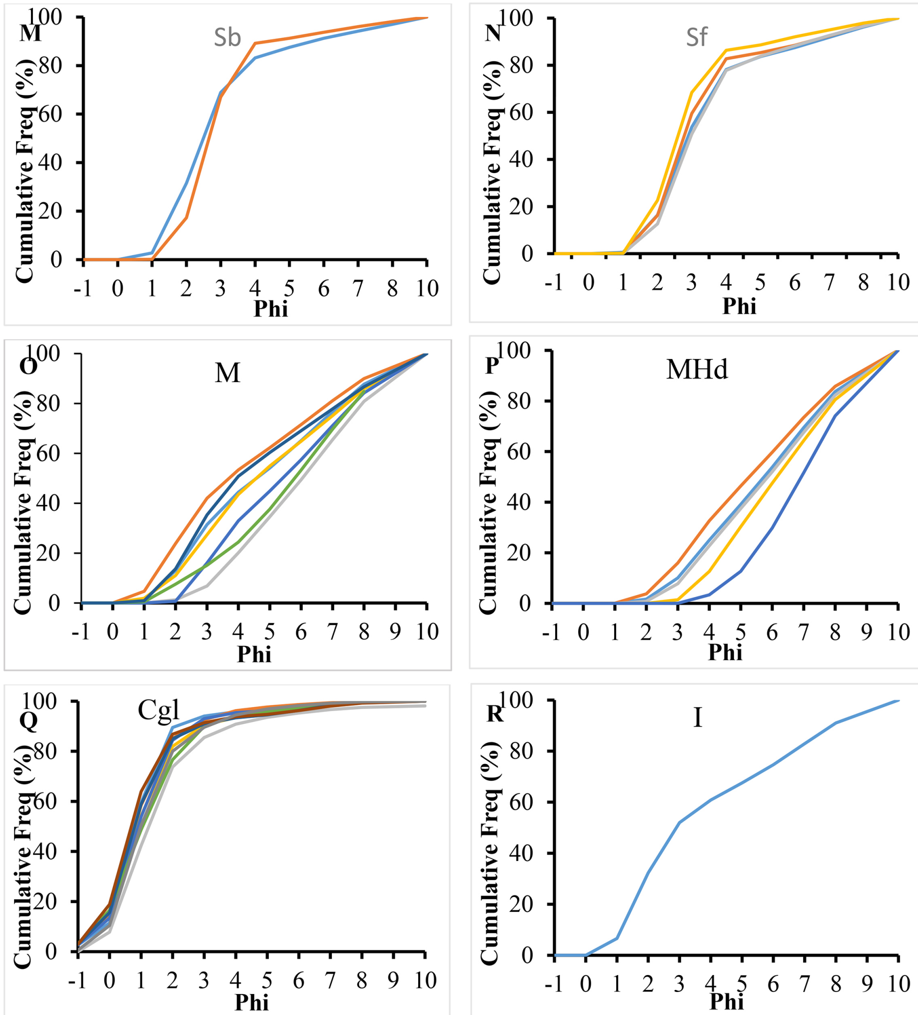

Figure 7. Cumulative frequency curves for facies of the study area: A) Irregularly Laminated Heterolithics, B) Planar Laminated Heterolithics, C) Sandy Heterolithics, D) Bioturbated Heterolithics, E) Muddy Debrite, F) Sandy Debrite, G) Ripple Cross-Laminated Sandstone, H Structureless Sandstone, I) Weakly Stratified Sandstone, J) Pebbly Sandstone, K) Planar Stratified Sandstone, L) Dewatered/Deformed Sandstone, M) Bioturbated Sandstone, N) Fine Grained Sandstone, O) Mudstone, P) Slump Deformed Mudstones/Heterolithics, Q) Conglomerate and R) Injectite.

6.3. Sediment Classification

On the Folk (1954, 1974) sediment classification ternary diagram, the samples generally form a tight grouping along the sand, silty sand and sandy silt side for the fine plot. Of the 18 samples, one, (Sm) about 6% of the total is classified as sand, eight others (Sb, Sf, Sp, Sxr, Hs, I, Hb and Dm) which is about 44% are classified as silty sand and four samples, (Hp, Hi, M, MHd) making up 22% of the sample total are classified as sandy silt (**Figure 8(A)**).

For the coarse plot, four samples, (Cgl, Sc, Sd and Ss) about 22% grouped around slightly gravelly sand with only one sample (Ds) constituting 6%, plotted in the gravelly muddy sand (**Figure 8(B)**).

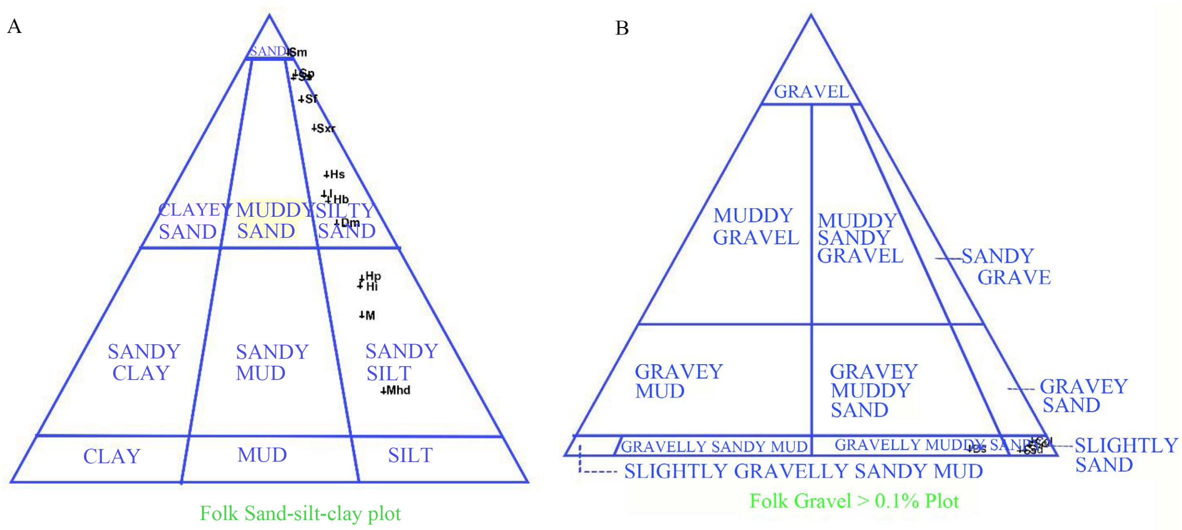

Figure 8. Ternary diagrams of sediment classification scheme from Folk (1954, 1974), Produced by program SEDPLOT: A) samples with no gravel and B) samples with GREATER THAN 0.1% gravel.

On the Shepard (1954) sediment classification ternary diagram, the samples generally form a tight grouping along the sand, silt and clay (gravel < 10%) side for the coarse plot. Of the 18 samples, five samples, (Cgl, Ss, Sc, Sd and Ds) constituting 28% plotted in the sand, silt and clay (gravel <10%) region (**Figure 9(A)**).

For the fine plot, four samples, (Hi, Hp, MHd and M) about 22.2% grouped around sandy silt, additional four, (Hb, Hs, Dm and I) which makes up 22.2% of the samples plotted in the silty sand portion with ten other samples (Sb, Sd, Sf, Sc, Sp, Sxr, Ss, Sm, Ds and Cgl) which is about 55.6% grouping in the sand region (**Figure 9(B)**).

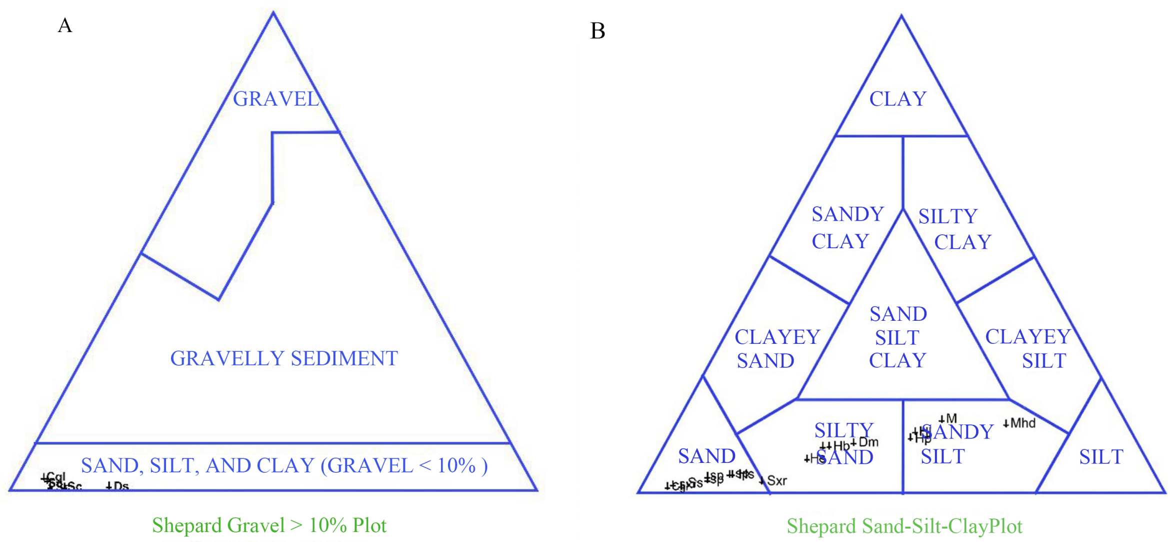

Figure 9. Ternary diagrams of sediment classification scheme from Shepard (1954) and modified by Schlee (1973), produced by program SEDPLOT: a) samples with gravel and b) samples with no gravel.

6.4. Statistical Parameters—Moment Measures

According to the graphic median, at a given value, half of the particles are coarser and the other half are finer. The values in this sample range from 0.87 to 6.09, with an average of 2.91 (**Table 2**) which shows that the grains are typically fine. The median class yielded several fairly high results, indicating that the sediments are abundant in a particular grain size.

The results of the mean demonstrates that the reservoir unit is primarily composed of medium to silt sand deposits, with a range of 1.01 to 6.29 and an average of 3.26 (**Table 2**). According to Ghaznavi et al. (2019), the peculiar size distribution of very fine sand may be the result of the low energy environment that occurred at the time of deposition. The results of some samples, such as MHd, M, Hp, Hi, Hb, Hs and Dm (**Figure 10(A)**) are relatively high since that kind of sediment class predominates. On the other hand, some samples such as Cgl, Sc, Sm, Sd and Ss (**Figure 10(A)**) however, is low because there are about equally many fine and very fine sediments, and they are poorly sorted since there is a large variation in grain size.

Table 2. Results for moment statistical parameters using GSSTAT software.

Depth (m)	Facies	Median	Mean	Standard Deviation	Skewness	Kurtosis
3421.50 - 3474.80	Dewatered/deformed sandstone (Sd)	1.26	1.41	1.57	0.32	1.55
3465.50 - 3503.91	Pebbly sandstone (Sc)	0.96	1.14	1.45	0.34	1.56
3298.10 - 3410.50	Sandy heterolithics (Hs)	3.40	4.12	2.14	0.55	1.19
3401.50 - 3466.50	Structureless sandstone (Ss)	1.64	1.77	1.50	0.30	1.45
3393.50 - 3492.70	Mudstone (M)	5.22	5.27	2.53	0.06	0.82
3394.50 - 3462.54	Irregularly laminated heterolithics (Hi)	4.61	4.89	2.66	0.14	0.93
3396.50 - 3483.50	Slump deformed mudstones/heterolithics (MHd)	6.09	6.29	2.36	0.07	0.85
3403.05 - 3404.20	Muddy debrite (Dm)	3.56	4.08	2.78	0.29	0.81
3406.25 - 3504.50	Planar laminated heterolithics (Hp)	4.44	5.00	2.27	0.37	0.87
3407.42 - 3484.25	Ripple cross-laminated sandstone (Sxr)	3.22	3.62	1.61	0.49	1.78
3408.50 - 3502.50	Planar stratified sandstone (Sp)	2.53	2.54	1.59	0.17	1.66
3414.50 - 3479.50	Sandy debrite (Ds)	1.65	2.30	2.23	0.51	1.32
3419.05 - 3499.50	Weakly stratified sandstone (Sm)	1.26	1.40	1.56	0.35	1.85
3425.50 - 3434.50	Conglomerate (Cgl)	0.87	1.01	1.27	0.29	1.60
3439.50 - 3495.50	Bioturbated sandstone (Sb)	2.56	2.71	1.38	0.38	1.87
3450.57	Injectite (I)	2.87	3.82	2.70	0.51	0.80
3468.50 - 3505.50	Bioturbated heterolithics (Hb)	3.44	4.20	2.47	0.46	0.93
3500.55 - 3506.60	Fine grained sandstone (Sf)	2.78	3.12	1.60	0.48	1.85
	Average	2.91	3.26	1.98	0.34	1.32

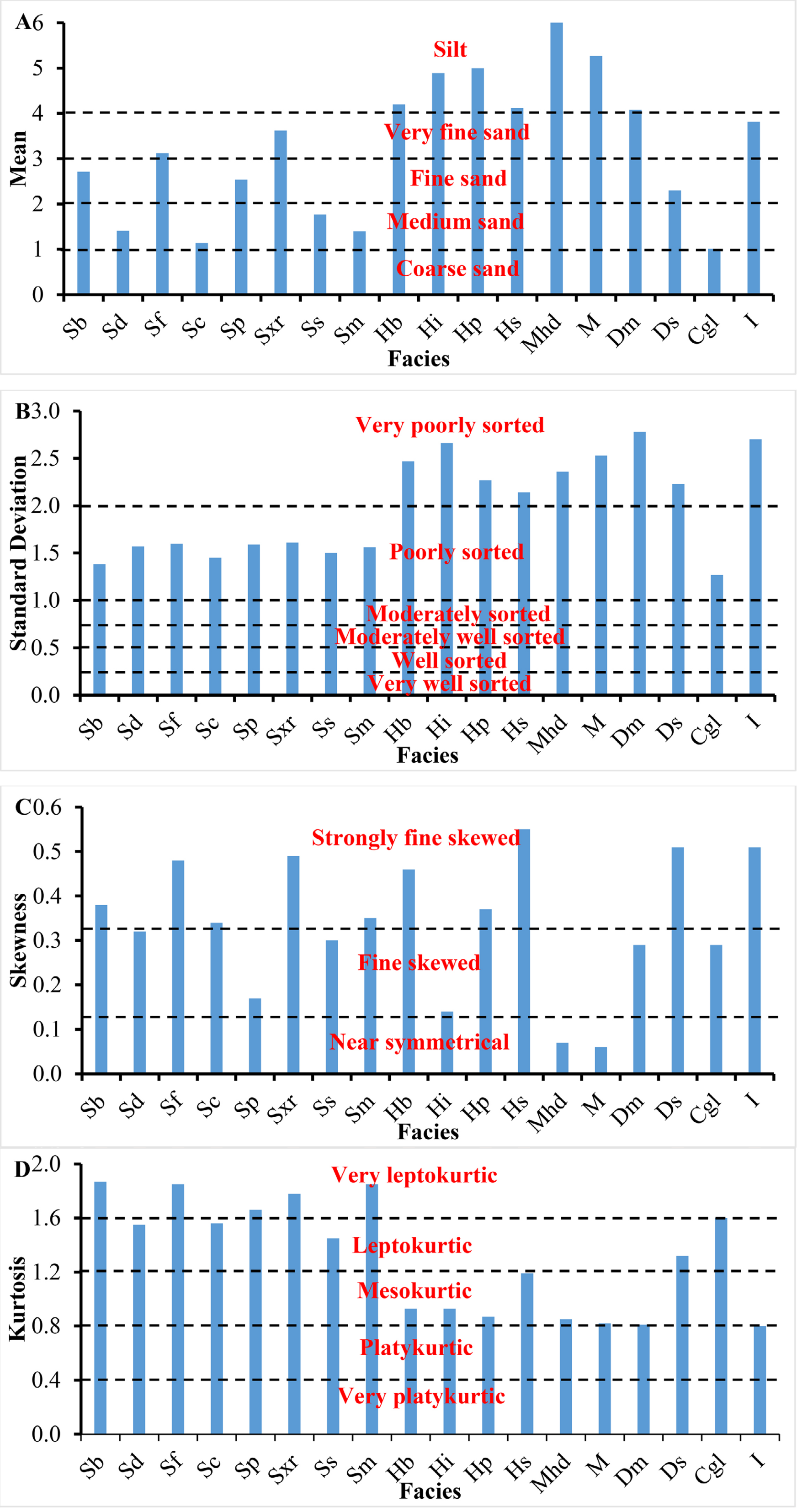

Figure 10. Histograms plotted with respect to the moment method: A) mean size, B) standard deviation, C) skewness and D) kurtosis.

Standard Deviation assesses the homogeneity or sorting of the grains, which reveals the energy conditions present during transport and deposition. Majority of the samples denotes poor sorting, with only a few other samples, Hb, Hi, Hp, Hs, MHd, M, Dm, Ds and I showing very poor sorting (**Figure 10(B)**). It ranges from 1.27 to 2.78 with a mean of 1.98 (**Table 2**). The poorly sorted sediments show a mixing of sediments of different sizes as well as a little variation in the mode of transporting current velocity. Although it reflects the energy state of the environment of deposition (Ghaznavi et al., 2019), it does not primarily assess the degree to which the sediment has been mixed.

Skewness evaluates the degree of asymmetry in the frequency curves in terms of the dominance of fine or coarse-grained fractions and thus evident of deposition energy. The skewness values for the sand samples range from 0.06 to 0.55 with an average skewness of 0.34 (**Table 2**). Almost all the samples are very fine skewed or exhibits positive skewness, suggesting that the sample accumulated in a low-energy environment with only one sample, MHd being near symmetrical and M being fine skewed (**Figure 10(C)**). This denotes that a higher percentage of particles is present in the fine tail of the sediments.

Kurtosis denotes the sharpness of the grain size frequency distribution which compares sorting of the middle portion to the tail spread and indicates whether the distribution is relatively narrow and peaked (leptokurtic) or broad and flat (platykurtic). With an average value of 1.32, the peak of the samples ranges from 0.80 to 1.87 (**Table 2**). The grains occupy the very leptokurtic zone with better sorting at the tails (**Figure 10(D)**).

6.5. Interrelationship of Size Parameters

Based on the presumption that distinct depositional settings represent various fluid mechanisms for sediment transport and deposition, bivariate plots are produced to discriminate between them (Sutherland & Lee, 1994). The majority of the sample clusters in the field of medium and silt sand grains and are very poorly sorted to poorly sorted as shown by the mean size and standard deviation plot (**Figure 11(A)**). The very fine-grained sediments are an indication of low-energy conditions of deposition (Boggs, 2009).

The samples are clustered around very fine skewed and fine skewed, with an average mean value of 1.19, according to the bivariate plot between mean size and skewness (**Figure 11(B)**). They all lie in the fine and very fine skewed group but encircle in medium to silt grain sizes. According to Mean vs Kurtosis bivariate analysis indicates that the medium sand to silt grain sizes is scattered in platykurtic to very leptokurtic conditions (**Figure 11(C)**).

Standard deviation vs skewness plot shows that the very poorly sorted sediments are near symmetrical to strongly fine skewed in nature and the poorly sorted sediments are fine to very fine skewed (**Figure 11(D)**). Standard deviation vs kurtosis indicates that the very poorly sorted sediments are platykurtic to mesokurtic and poorly sorted sediments are leptokurtic to very leptokurtic in nature

(Figure 11(E)) and the skewness vs kurtosis plot exhibits near symmetrical to very fine skewing, revealing the sediment are scattered in the very platykurtic to very leptokurtic regions (Figure 11(F)).

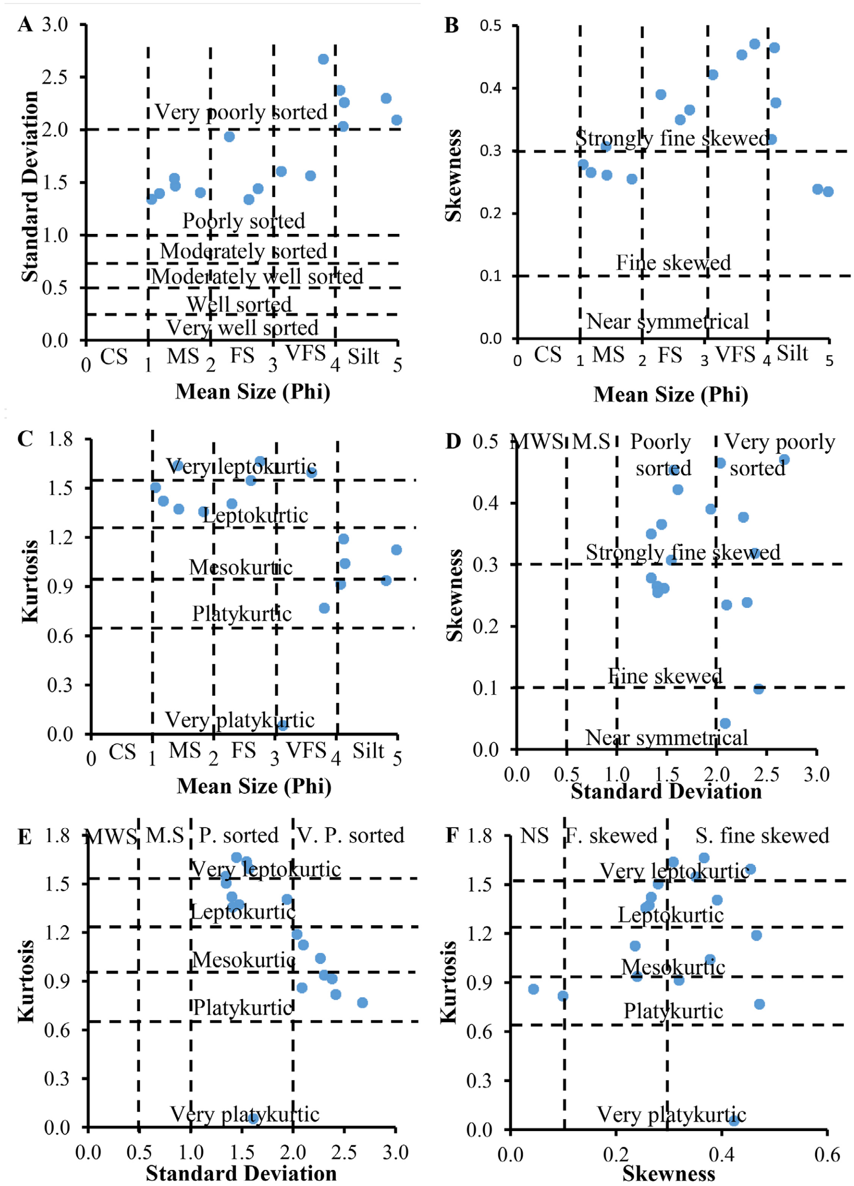

Figure 11. Bivariate plots between: A) mean and standard deviation, B) mean and skewness, C) mean and kurtosis, D) sorting and kurtosis, E) sorting and skewness and F) skewness and kurtosis; CS coarse sand, MS medium sand, FS fine sand, VFS, very fine sand, MWS moderately well sorted, M.S moderately sorted, ns near symmetrical.

6.6. Bivariate Grain Size Parameters

Bivariate is most successful at differentiating between beach and river sands as well as river and coastal dune sands according to (Moiola & Weiser, 1968) and (Azidane et al., 2021), and whether quarter, half, or whole phi data are employed, the differentiation is accurate. Therefore, statistical values obtained using both graphical and moment approaches were shown in different bivariate diagrams to confirm the existing paleoenvironmental conditions. Friedman (1961, 1967) created a bivariate by graphing skewness vs standard deviation to discriminate between beach and river sedimentary environments. The sample points plotted in the river (fluvial) environment when the graphical and moment measures were used (**Figure 12(A)**). The distinction between coastal dune and river environments was further made using the bivariate between skewness and kurtosis by (Folk & Ward, 1957) and (Ghaznavi et al., 2019), which supported (Friedman's 1961, 1967) findings. Most of the sample plot in the river environment with only a few plotting in the coastal dune environment for both graphical and moment statistical measures (**Figure 12(B)**).

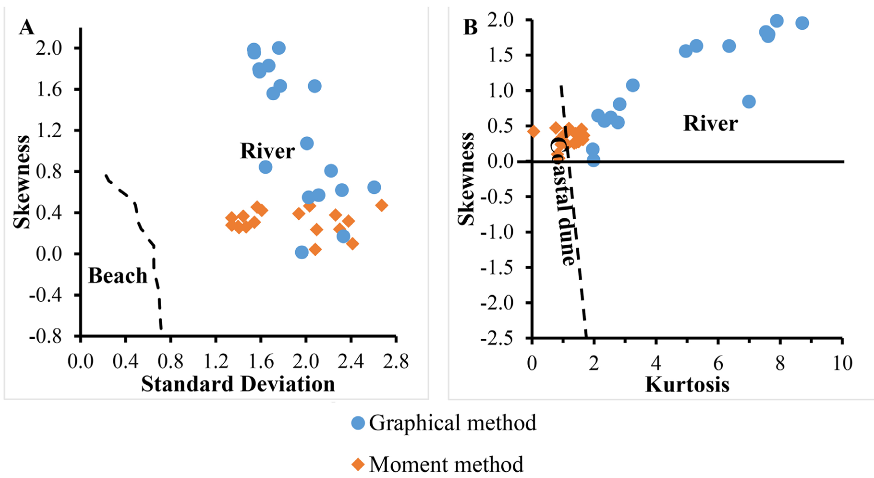

Figure 12. A) bivariate plot of skewness vs standard deviation (source: Friedman, 1967) and B) bivariate plot of skewness vs kurtosis (source: Folk & Ward, 1957).

6.7. Linear Discriminate Function (LDF) Analysis

Using (Equations (10)-(13)), it was discovered that Y1 demonstrated that each sample belongs to the beach environment after the linear discriminate function values were calculated using statistical parameters obtained by the graphical technique (**Table 3**). All of the sediments are shallow marine sediments with Hb and Sf being beach sediments, according to Y2 values. Y3 was used to compare the fluvial and shallow-marine predominance, and it was found that the former predominated. According to Y4, the sediments were primarily deposited by turbidity current with only Sf being fluvial in nature.

Table 3. Results of linear discriminate function analysis using the graphical method.

Depth (m)	Facies	Y1	Env	Y2	Env	Y3	Env	Y4	Env
3421.50 - 3474.80	Dewatered/deformed sandstone (Sd)	6.84	B	197.74	SM	−20.19	F	10.95	MT
3465.50 - 3503.91	Sandy heterolithics (Hs)	3.38	B	366.85	SM	−37.31	F	14.07	MT
3298.10 - 3410.50	Pebbly sandstone (Sc)	7.23	B	183.18	SM	−18.73	F	10.99	MT
3401.50 - 3466.50	Mudstone (M)	5.95	B	489.84	SM	−51.36	F	11.30	MT

Continued

3393.50 - 3492.70	Irregularly laminated heterolithics (Hi)	5.42	B	454.62	SM	−47.44	F	12.24	MT
3394.50 - 3462.54	Slump deformed mudstones/heterolithics (MHd)	−2.71	B	399.05	SM	−36.84	F	10.97	MT
3396.50 - 3483.50	Muddy debrite (Dm)	8.73	B	459.99	SM	−50.17	F	12.22	MT
3403.05 - 3404.20	Planar laminated heterolithics (Hp)	1.61	B	393.18	SM	−38.37	F	12.92	MT
3406.25 - 3504.50	Ripple cross-laminated sandstone (Sxr)	0.47	B	258.39	SM	−23.05	F	15.10	MT
3407.42 - 3484.25	Structureless sandstone (Ss)	4.88	B	195.19	SM	−18.91	F	11.07	MT
3408.50 - 3502.50	Planar stratified sandstone (Sp)	1.76	B	199.28	SM	−17.37	F	13.19	MT
3414.50 - 3479.50	Sandy debrite (Ds)	11.06	B	347.21	SM	−38.29	F	13.43	MT
3419.05 - 3499.50	Weakly stratified sandstone (Sm)	8.52	B	219.33	SM	−22.55	F	12.75	MT
3425.50 - 3434.50	Conglomerate (Cgl)	7.15	B	169.39	SM	−17.02	F	11.34	MT
3439.50 - 3495.50	Bioturbated sandstone (Sb)	2.42	B	219.29	SM	−19.45	F	14.12	MT
3450.57	Injectite (I)	14.30	B	551.52	SM	−63.75	F	12.86	MT
3468.50 - 3505.50	Bioturbated heterolithics (Hb)	6.95	B	−46.16	B	−46.16	F	13.14	MT
3500.55 - 3506.60	Fine grained sandstone (Sf)	−2.23	B	−23.95	B	−23.95	F	6.44	F
	Average	5.10	B	279.66	SM	−32.83	F	12.17	MT

B Beach, SM Shallow Marine, F Fluvial, T Marine Turbidity Current

The application of moment-method statistical parameters to the Linear Discriminant Function (Table 4) yielded consistent results. Y1 classified all samples as beach deposits while Y2 indicated a shallow-marine setting. Additionally, Y3 demonstrated the fluvial nature of the sediments, and Y4 was used to discriminate between fluvial and marine (turbidity current) environments. It showed that the marine turbidity environment predominated, with seven samples (Hb, Hi, Hp, MHd, M, Dm, and Cgl) classified as fluvial origin.

Table 4. Results of linear discriminate function analysis using the moment method.

Depth (m)	Facies	Y1	Env	Y2	Env	Y3	Env	Y4	Env
3421.50 - 3474.80	Dewatered/deformed sandstone (Sd)	8.25	B	218.51	SM	−22.68	F	10.38	MT
3465.50 - 3503.91	Sandy heterolithics (Hs)	4.81	B	397.39	SM	−41.58	F	11.13	MT
3298.10 - 3410.50	Pebbly sandstone (Sc)	7.87	B	191.02	SM	−19.68	F	10.52	MT
3401.50 - 3466.50	Mudstone (M)	7.31	B	519.35	SM	−54.83	F	5.97	F
3393.50 - 3492.70	Irregularly laminated heterolithics (Hi)	11.34	B	561.22	SM	−61.23	F	6.54	F
3394.50 - 3462.54	Slump deformed mudstones/heterolithics (MHd)	0.67	B	481.43	SM	−47.30	F	7.26	F
3396.50 - 3483.50	Muddy debrite (Dm)	15.97	B	591.93	SM	−67.92	F	6.07	F
3403.05 - 3404.20	Planar laminated heterolithics (Hp)	3.17	B	439.66	SM	−45.48	F	8.63	F
3406.25 - 3504.50	Ripple cross-laminated sandstone (Sxr)	1.20	B	268.80	SM	−23.99	F	14.29	MT
3407.42 - 3484.25	Structureless sandstone (Ss)	5.90	B	207.82	SM	−20.60	F	10.06	MT
3408.50 - 3502.50	Planar stratified sandstone (Sp)	5.11	B	239.67	SM	−22.17	F	10.74	MT
3414.50 - 3479.50	Sandy debrite (Ds)	13.25	B	396.43	SM	−45.34	F	10.07	MT

Continued

3419.05 - 3499.50	Weakly stratified sandstone (Sm)	9.05	B	222.39	SM	−22.54	F	12.18	MT
3425.50 - 3434.50	Conglomerate (Cgl)	6.75	B	156.65	SM	−15.18	F	10.50	MT
3439.50 - 3495.50	Bioturbated sandstone (Sb)	2.41	B	209.04	SM	−17.68	F	13.64	MT
3450.57	Injectite (I)	14.78	B	562.85	SM	−65.23	F	7.49	F
3468.50 - 3505.50	Bioturbated heterolithics (Hb)	9.53	B	492.17	SM	−54.45	F	8.59	F
3500.55 - 3506.60	Fine grained sandstone (Sf)	3.10	B	259.98	SM	−23.80	F	14.24	MT
	Average	7.25	B	356.46	SM	−37.32	F	9.91	F

B Beach, SM Shallow Marine, F Fluvial, T Marine Turbidity Current

The LDF plot of Y1 versus Y2 plot (Figure 13(A)) shows that the majority of samples plot in the Beach shallow agitated field, with only three samples departing into the aeolian or littoral fields. Similarly, the Y2 versus Y3 plot (Figure 13(B)) places nearly all samples in the Shallow marine agitated field, with two samples plotting as Fluvial beach. The Y3 vs Y4 plot (Figure 13(C)) shows that all samples, from both the graphical and moment techniques, fall inside the Fluvial/Turbidity current field, with no samples falling in the purely fluvial or shallow marine fields. This suggests that the sediments originated from a fluvial sand population but were eventually deposited by turbidity-current (sediment gravity flow) processes, indicating a deep-water turbidite system fed by a fluvial frontier rather than a beach or shallow-marine reworking pathway.

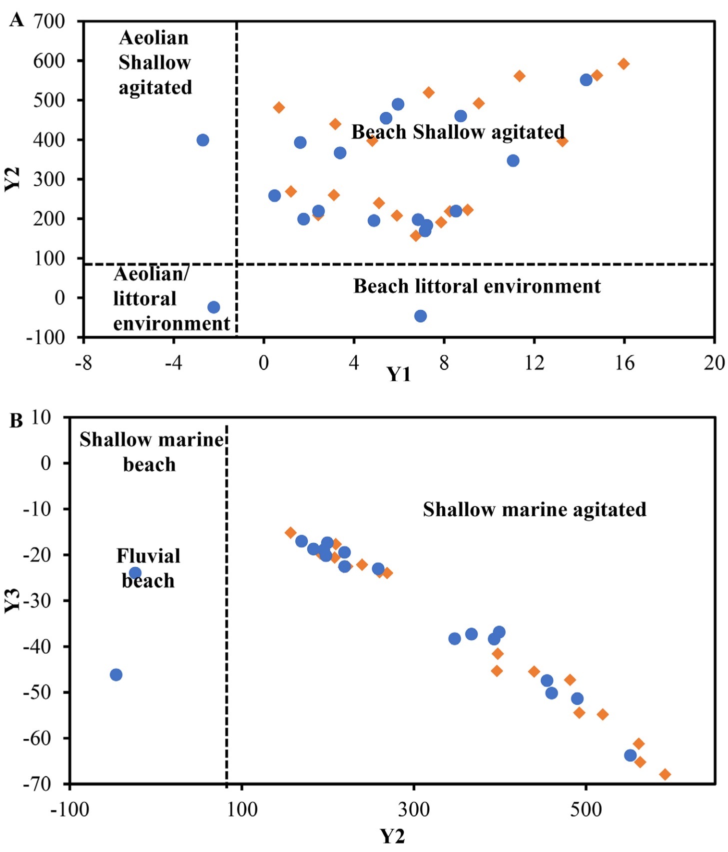

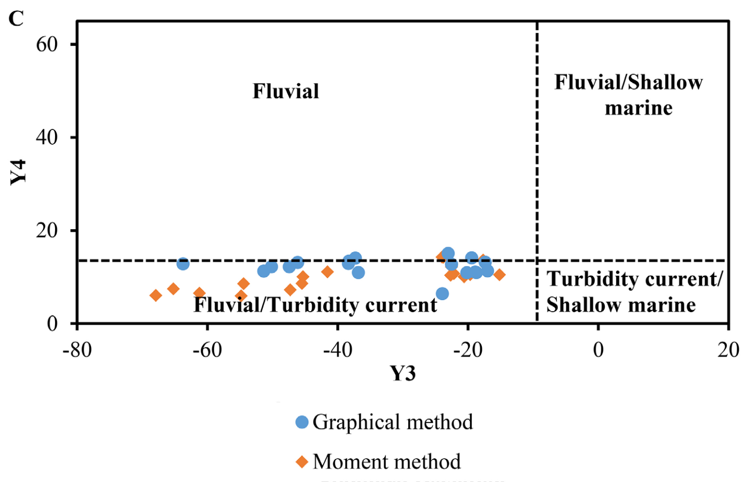

Figure 13. Linear discriminate function plot for the study area: A) Y1 vs Y2, B) Y2 vs Y3 and C) Y3 vs Y4.

7. Conclusions

The following findings were drawn from the study of grain size data from one hundred and forty-one samples of the Jubilee Field in the Turonian interval.

The grain size statistics and cumulative frequency curves reflect the relatively very fine-grained character of the sediments. Most of the sample population was transported via saltation, followed by the suspension process and very few indications of the traction process.

The LDF bivariate plot indicates that the sand in the studied facies is texturally mature, characterised by being well sorted and rounded, typical of reworking in a beach or shallow-marine environment. The sands were ultimately remobilised and redeposited via turbidity currents, indicating a sediment-gravity-flow transport mechanism, while also showing a textural characteristic of shallow marine deposition.

The facies of the Jubilee Field were Irregularly Laminated Heterolithics, Planar Laminated Heterolithics, Sandy Heterolithics, Bioturbated Heterolithics, Muddy Debrite, Sandy Debrite, Ripple Cross-Laminated Sandstone, Structureless Sandstone, Weakly Stratified Sandstone, Pebbly Sandstone, Planar Stratified Sandstone, Dewatered/Deformed Sandstone, Bioturbated Sandstone, Fine Grained Sandstone, Mudstone, Slump Deformed Mudstones/Heterolithics, Conglomerate and Injectite based on the lithology.

Conflicts of Interest

The authors declare no conflicts of interest regarding the publication of this paper.

References

Anon (2009). *Jubilee Field—Ghana—Offshore Technology.* https://www.offshore-technology.com/projects/jubilee-field/

Ansah, E., Ewusi, A., Brantson, E. T., Kuma, J. S. Y., Opeloye, S. A., Obeng, B. K. et al.

(2022). Sedimentological and Facies Characterization in the Modelling of the Turonian Sandstone Reservoir Package, Jubilee Field, Ghana. *Modeling Earth Systems and Environment, 9,* 1135-1168. https://doi.org/10.1007/s40808-022-01550-z

Antobreh, A. A., Faleide, J. I., Tsikalas, F., & Planke, S. (2009). Rift-Shear Architecture and Tectonic Development of the Ghana Margin Deduced from Multichannel Seismic Reflection and Potential Field Data. *Marine and Petroleum Geology, 26,* 345-368. https://doi.org/10.1016/j.marpetgeo.2008.04.005

Atat, J. G., Akpabio, I. O., & Ekpo, S. S. (2022). Percentile-Oqive Approach Determines the Textural Parameters of Xa Field Lithology and the Suitable Technique for Porosity Estimates. *Current Science, 2,* 230-240.

Atta-Peters, D., Agama, C. I., Asiedu, D. K., & Apesegah, E. (2013). Palynology, Palynofacies and Palaeoenvironments of Sedimentary Organic Matter from Bonyere-1 Well, Tano Basin, Western Ghana. *International Letters of Natural Sciences, 5,* 27-45. https://doi.org/10.56431/p-i2vlvk

Azidane, H., Michel, B., Bouhaddioui, M. E., Haddout, S., Magrane, B., & Benmohammadi, A. (2021). Grain Size Analysis and Characterization of Sedimentary Environment along the Atlantic Coast, Kenitra (Morocco). *Marine Georesources & Geotechnology, 39,* 569-576. https://doi.org/10.1080/1064119x.2020.1726536

Baiyegunhi, T. L., Liu, K., Gwavava, O., & Baiyegunhi, C. (2020). Textural Characteristics, Mode of Transportation and Depositional Environment of the Cretaceous Sandstone in the Bredasdorp Basin, off the South Coast of South Africa: Evidence from Grain Size Analysis. *Open Geosciences, 12,* 1512-1532. https://doi.org/10.1515/geo-2020-0135

Bempong, F. K., Ehinola, O., Apesegah, E., Hotor, V. K., & Botwe, K. (2021). Sequence Stratigraphic Framework, Depositional Settings and Hydrocarbon Prospectivity of the Campanian Section, Tano Basin Southwestern Ghana. *Petroleum and Coal, 63,* 204-215.

Bempong, F. K., Ehirim, C. N., Takyi, B., Addai, C. M., Sarkodie, K., & Akaba, P. A. (2022). A Stratigraphic Discuss on the Current Knowledge of the Tano Basin: From Shallow Waters to Deep Waters. In *Proceedings of 7th UMaT Biennial International Mining and Mineral Conference* (12 p).

Bempong, F. K., Ozumba, B. M., Hotor, V., Takyi, B., & Nwanjide, C. S. (2019). A Review of the Geology and the Petroleum Potential of the Cretaceous Tano Basin of Ghana. *Journal of Petroleum and Environmental Biotechnology, 10,* 8.

Boggs Jr., S. (2009). *Petrology of Sedimentary Rocks* (2nd ed., pp. 67-98). Cambridge University Press. https://doi.org/10.1017/cbo9780511626487

Cheng, W., Chen, S., Zhu, J., Zhong, X., Hu, J., & Guo, J. (2023). Identification of the Sediment Movement Mechanism via Grain Size and Shape: A Case Study of a Beach in Eastern Hainan Island in South China. *Water, 15,* Article No. 3637. https://doi.org/10.3390/w15203637

Dailly, P., Henderson, T., Hudgens, E., Kanschat, K., & Lowry, P. (2013). Exploration for Cretaceous Stratigraphic Traps in the Gulf of Guinea, West Africa and the Discovery of the Jubilee Field: A Play Opening Discovery in the Tano Basin, Offshore Ghana. *Geological Society, London, Special Publications, 369,* 235-248. https://doi.org/10.1144/sp369.12

Folk, R. L. (1954). The Distinction between Grain Size and Mineral Composition in Sedimentary-Rock Nomenclature. *The Journal of Geology, 62,* 344-359.

Folk, R. L. (1974). *Petrology of Sedimentary Rocks* (182 p). Hemphill Publishing Company Austin.

Folk, R. L., & Ward, W. C. (1957). Brazos River Bar [Texas]; a Study in the Significance of

Grain Size Parameters. *Journal of Sedimentary Research, 27,* 3-26. https://doi.org/10.1306/74d70646-2b21-11d7-8648000102c1865d

Friedman, G. M. (1961). Distinction between Dune, Beach, and River Sands from Their Textural Characteristics. *Journal of Sedimentary Research, 31,* 514-529. https://doi.org/10.1306/74d70bcd-2b21-11d7-8648000102c1865d

Friedman, G. M. (1967). Dynamic Processes and Statistical Parameters Compared for Size Frequency Distribution of Beach and River Sands. *Journal of Sedimentary Research, 37,* 327-354. https://doi.org/10.1306/74d716cc-2b21-11d7-8648000102c1865d

Ghaznavi, A. A., Quasim, M. A., Ahmad, A. H. M., & Ghosh, S. K. (2019). Granulometric and Facies Analysis of Middle-Upper Jurassic Rocks of Ler Dome, Kachchh, Western India: An Attempt to Reconstruct the Depositional Environment. *Geologos, 25,* 51-73. https://doi.org/10.2478/logos-2019-0005

Kanhaiya, S., Singh, B. P., Tripathi, M., Sahu, S., & Tiwari, V. (2017). Lithofacies and Particle-Size Characteristics of Late Quaternary Floodplain Deposits along the Middle Reaches of the Ganga River, Central Ganga Plain, India. *Geomorphology, 284,* 220-228. https://doi.org/10.1016/j.geomorph.2016.08.030

Krumbein, W. C., & Pettijohn, F. J. (1938). *Manual of Sedimentary Petrography* (549 p). Appleton Century.

López, G. I. (2017). Grain Size Analysis. In A. S. Gilbert (Ed.), *Encyclopedia of Geoarchaeology* (pp. 341-348). Springer. https://doi.org/10.1007/978-1-4020-4409-0_18

Moiola, R. J., & Weiser, D. (1968). Textural Parameters; an Evaluation. *Journal of Sedimentary Research, 38,* 45-53. https://doi.org/10.1306/74d718c5-2b21-11d7-8648000102c1865d

Nichols, G. (2009). *Sedimentology and Stratigraphy* (2nd ed.). Blackwell Scientific Publications.

Ocheli, A., Okoro, A. U., Ogbe, O. B., & Aigbadon, G. O. (2018). Granulometric and Pebble Morphometric Applications to Benin Flank Sediments in Western Anambra Basin, Nigeria: Proxies for Paleoenvironmental Reconstruction. *Environmental Monitoring and Assessment, 190,* 1-17. https://doi.org/10.1007/s10661-018-6637-z

Ogbe, O. B. (2021). Reservoir Sandstone Grain-Size Distributions: Implications for Sequence Stratigraphic and Reservoir Depositional Modelling in Otovwe Field, Onshore Niger Delta Basin, Nigeria. *Journal of Petroleum Science and Engineering, 203,* Article ID: 108639. https://doi.org/10.1016/j.petrol.2021.108639

Oyanyan, R. O., & Olugun, A. K. (2023). Depositional Environments and Reservoir Quality Potentials of Campanian Sediments at Macgregor, Afikpo Basin, Nigeria. *International Journal of Earth Sciences Knowledge and Applications, 5,* 62-78.

Poppe, L. J., & Eliason, A. H. (2008). A Visual Basic Program to Plot Sediment Grain-Size Data on Ternary Diagrams. *Computers & Geosciences, 34,* 561-565. https://doi.org/10.1016/j.cageo.2007.03.019

Poppe, L. J., Eliason, A. H., & Hastings, M. E. (2004). A Visual Basic Program to Generate Sediment Grain-Size Statistics and to Extrapolate Particle Distributions. *Computers & Geosciences, 30,* 791-795. https://doi.org/10.1016/j.cageo.2004.05.005

Rüpke, L. H., Schmid, D. W., Hartz, E. H., & Martinsen, B. (2010). Basin Modelling of a Transform Margin Setting: Structural, Thermal and Hydrocarbon Evolution of the Tano Basin, Ghana. *Petroleum Geoscience, 16,* 283-298. https://doi.org/10.1144/1354-079309-905

Sahu, B. K. (1964). Depositional Mechanisms from the Size Analysis of Clastic Sediments. *Journal of Sedimentary Research, 34,* 73-83.

https://doi.org/10.1306/74d70fce-2b21-11d7-8648000102c1865d

Schlee, J. S. (1973). *Atlantic Continental Shelf and Slope of the United States—Sediment Texture of the Northeastern Part* (Vol. 529-L, 64 p). US Geological Survey Professional Paper, The United States Geological Survey (USGS).

Shepard, F. P. (1954). Nomenclature Based on Sand-Silt-Clay Ratios. *Journal of Sedimentary Research, 24,* 151-158. https://doi.org/10.1306/d4269774-2b26-11d7-8648000102c1865d

Sutherland, R. A., & Lee, C. (1994). Discrimination between Coastal Subenvironments Using Textural Characteristics. *Sedimentology, 41,* 1133-1145. https://doi.org/10.1111/j.1365-3091.1994.tb01445.x

Tullow Ghana Limited (2019). *TEN Field*. https://www.tullowoil.com/operations/westafrica/ghana/ten-field

Visher, G. S. (1969). Grain Size Distributions and Depositional Processes. *Journal of Sedimentary Research, 39,* 1074-1106. https://doi.org/10.1306/74d71d9d-2b21-11d7-8648000102c1865d